INORGANIC CHEMISTRY
FRONTIERS

RESEARCH ARTICLE

View Article Online
View Journal | View Issue

Cite this: *Inorg. Chem. Front.*, 2024, **11**, 4802

A dual approach to cancer treatment: gold(I) terpyridine derivatives as DNA binders and inhibitors of mammalian thioredoxin reductase†

María Gil-Moles,[a,b,c] M. Elena Olmos,[b] José M. López-de-Luzuriaga,*[b] Ingo Ott*[c] and M. Concepción Gimeno*[a]

Gold(I) complexes featuring a phosphine-substituted terpyridine (4′-PPh_2terpy), along with various ancillary ligands, have been successfully synthesised. All derivatives, characterised by the general formula [Au(L)(4′-PPh_2terpy)] (where L represents phosphine, chloride, alkynyl, or thiolate), exhibit remarkable activity against diverse tumour cell lines, including HT-29, MCF-7, and MDA-MB-231, with particularly noteworthy efficacy against the triple negative breast cancer MDA-MB-231 cell line. Notably, all complexes demonstrate superior efficacy compared to the reference auranofin, showcasing IC_{50} values ten-fold lower. Additionally, they exhibit a certain level of selectivity towards healthy cells (primary fibroblasts). The ability of different ancillary ligands to undergo ligand exchange reactions with thiol groups, such as NAC, has been assessed *via* NMR. A correlation between the leaving group capacities of various ligands and the speed of ligand exchange reactions has been observed, following this order: alkynyl < phosphine < thiolate < chloride. Moreover, efforts were made to elucidate potential biological targets and the underlying mechanism of action through which these Au(I) compounds impede cell proliferation. Flow cytometry measurements have indicated several cellular responses, including apoptotic cell death, cell cycle arrest in the G0/G1 phase, increased ROS production, and a decrease in mitochondrial membrane potential ($\Delta\Psi$). DNA binding studies revealed that the selected derivatives interact with DNA by intercalation. Additionally, investigations on the inhibition of the TrxR system yielded compelling findings. The Au(I) complexes exhibited potent enzyme inhibition, albeit variations were noted based on the ancillary ligand employed. A clear correlation emerged between the inhibition observed and the capability to displace the ancillary ligand with the selenol moieties of TrxR (the effectiveness follows the same order as observed in the study of ligand exchange reactions). Notably, the chloride ligand yielded the most promising results, demonstrating inhibition levels comparable to auranofin, one of the foremost TrxR inhibitors. This suggests a dual approach for cancer therapy with complexes targeting two key biological targets.

Received 24th March 2024,
Accepted 20th June 2024
DOI: 10.1039/d4qi00755g
rsc.li/frontiers-inorganic

Introduction

In the last decades, there has been substantial progress in the fields of bioinorganic and medicinal chemistry. This advancement is largely credited to the remarkable pharmacological efficacy exhibited by metal derivatives in treating a wide array of diseases. In this regard, metallodrugs have revealed opportunities that are not accessible to pure organic molecules.[1] Platinum complexes, such as cisplatin, carboplatin, and oxaliplatin, have transformed cancer therapy globally,[2] despite accompanying several drawbacks, and consequently, there is a growing focus on exploring alternative metallic complexes and designing organic ligands for novel anticancer agents. Gold complexes, such as auranofin, which is approved for rheumatoid arthritis, have demonstrated promising anticancer properties in recent studies and is currently undergoing clinical trials for several types of cancer.[3] This has prompted the development of next-generation gold complexes for cancer treatment, with several examples showcasing excellent activity in both gold(I) and gold(III) complexes.[4–9]

The mechanisms of action of platinum and gold complexes initially appeared similar due to the structural resemblances of

[a]*Departamento de Química Inorgánica, Instituto de Síntesis Química y Catálisis Homogénea (ISQCH), CSIC-Universidad de Zaragoza, 50009 Zaragoza, Spain. E-mail: gimeno@unizar.es*
[b]*Departamento de Química, Universidad de La Rioja. Instituto de Investigación en Química (IQUR). Complejo Científico-Tecnológico, Madre de Dios 53, 26006-Logroño, Spain. E-mail: josemaria.lopez@unirioja.es*
[c]*Institute of Medicinal and Pharmaceutical Chemistry, Technische Universität Braunschweig, Beethovenstr. 55, 38106 Braunschweig, Germany. E-mail: ingo.ott@tu-bs.de*

† Electronic supplementary information (ESI) available. See DOI: https://doi.org/10.1039/d4qi00755g

Pt(II) and Au(III). However, subsequent research has revealed significant differences. Instead of targeting DNA like platinum, gold compounds were found to rapidly interact with thiols in proteins such as albumin, immunoglobulins, and enzymes like TrxR (thioredoxin reductase), GR (glutathione reductase), caspases such as cysteine protease, or PTP (protein tyrosine phosphatases). Gold coordinates to the active sites of these enzymes, either inhibiting them or altering their three-dimensional structure, leading to beneficial therapeutic effects.[2,4–8]

Functionalised terpyridine derivatives serve as prominent ligands within coordination chemistry. Notably, metal compounds incorporating such ligands exhibit intriguing properties as anticancer agents. Terpyridine complexes, in particular, demonstrate efficient DNA intercalation and manifest inhibitory activity against cancer cells *in vitro*.[10–12] Although some studies have investigated Au(III) derivatives of terpyridine, research on Au(I) counterparts remains limited, with negligible exploration into their biological properties.[13–17] The scarcity of Au(I)-terpy compounds may be attributed to the moderate affinity of Au(I) centres for nitrogen. Consequently, the majority of Au(I)-terpy compounds observed are stabilised with ancillary ligands such as phosphines or perhalophenyl groups, which facilitate the stabilisation of these compounds.[18–20]

In this study, we have undertaken the synthesis of various Au(I) derivatives featuring terpyridine-type ligands. Notably, we have introduced a diphenylphosphino group at the 4′ position of the terpyridine ligand (4′-PPh_2terpy), as depicted in Fig. 1. The incorporation of this phosphine facilitates that the coordination of phosphorus instead of nitrogen to the gold centre enhances their stabilities in solution.

As previously discussed, terpyridine-derived ligands are known to promote interactions with DNA, and the presence of the gold atom is expected to contribute to the inhibition of the TrxR system. Consequently, our research involves a comprehensive examination of these synthesised derivatives, encompassing their impact on cell proliferation, interactions with DNA, and their potential to inhibit the TrxR system, all of which are considered as potential biological targets.

Moreover, our investigation embraces the incorporation of various ancillary ligands, including phosphine, chloride, alkynyl, and nucleobase-derived thiolate ligands. The inclusion of these ancillary ligands aims to shed light on their influence on the interactions of the terpyridine-gold couple with the biomolecules.

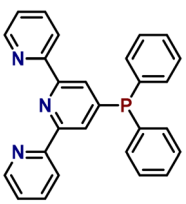

Fig. 1 Chemical structure of 4′-PPh_2terpy ligand.

Results and discussion

Synthesis and characterization

As previously outlined, our primary aim was to synthesise stable gold complexes utilizing terpyridine-containing ligands. To achieve this goal, we selected the terpyridine-phosphine ligand as the phosphine moiety will allow to form strong bonds with the gold centre through the phosphorous atom. Gold(I) complexes bearing the ligand 4-PPh_2terpy and phosphine as ancillary ligands, **1** and **2**, have been prepared by reaction of [AuCl(Ph_2R)] (R = Ph, C_6H_4(COOH)) in the presence of $AgBF_4$, as depicted in Scheme 1. The preparation of the Au(I) derivative with chloride as ancillary ligand [AuCl(4′-PPh_2terpy)] (**3**) was achieved by substitution of the labile tetrahydrothiophene (tht) ligand in [AuCl(tht)]. Additionally, substitution of the chloride ligand with terminal alkynes, such as phenylacetylene, 2-ethynylpyridine, phenyl-propargyl sulphide, provide complexes **4**, **5**, and **6**. Substitution with nucleobase-derived thiolates, such as 2-mercaptopyrimidine, 6-methylthiouracil or 2-thiocytosine, as ancillary ligands afford complexes **7**, **8**, and **9** (see Scheme 1).

All the complexes underwent thorough characterisation *via* elemental analysis, IR spectroscopy, ESI exact mass spectrometry, and NMR spectroscopy, as detailed in the Experimental section. The spectroscopic and analytical data consistently support the proposed stoichiometries. The ^{1}H NMR spectra of the new compounds display the expected resonances (see Experimental section and ESI†). Analysis of the ^{31}P$\{^1$H$\}$ NMR spectra of the gold(I) complexes indicates that the gold atom is bonded to the phosphorus atom of the 4′-PPh_2terpy ligand. In the case of compounds **1** and **2**, broad signals are observed at room temperature in both cases, appearing at 44.35 and 44.26 ppm, respectively. NMR experiments were performed at low temperature (220 K), due to the potential equilibrium with complexes of the [P–Au–P′]$^+$ type, which may exist in homoleptic and heteroleptic forms. In fact, analysis of the spectra indicates the presence of this equilibrium for complex **1**, which presents an AB system for the heteroleptic species and two overlapping singlets for the homoleptic ones; however, complex **2** exhibits two distinct doublets reflecting the presence of two inequivalent phosphorus atoms, corroborating that the structure remains stable in solution (see ESI Fig. S3 and S4†). The ^{31}P$\{^1$H$\}$ NMR spectra of **3** shows a weak signal at 33.23 ppm indicating that the gold atom is coordinated to the phosphorus centre, given the large chemical shift compared to the free ligand (δ = −5.10 ppm). Regarding ^{31}P$\{^1$H$\}$ NMR spectra of **4–6**, a resonance around 42 ppm is observed for all the complexes (42.17 (**4**), 42.24 (**5**) and 41.61 (**6**)). Compounds **7–9** exhibit a signal around 38 ppm (38.19 (**7**), 37.83 (**8**), 37.70 (**9**)) (see Experimental section and ESI Fig. S1–S9†). ESI(+) exact mass spectra in acetone were recorded and, in all cases, the isotopic distributions found experimentally agree with the theoretical ones. When the ancillary ligand used is a phosphine (**1** and **2**), the peaks corresponding to heteroleptic and homoleptic complexes were detected (see Experimental section). The other complexes (**3–9**)

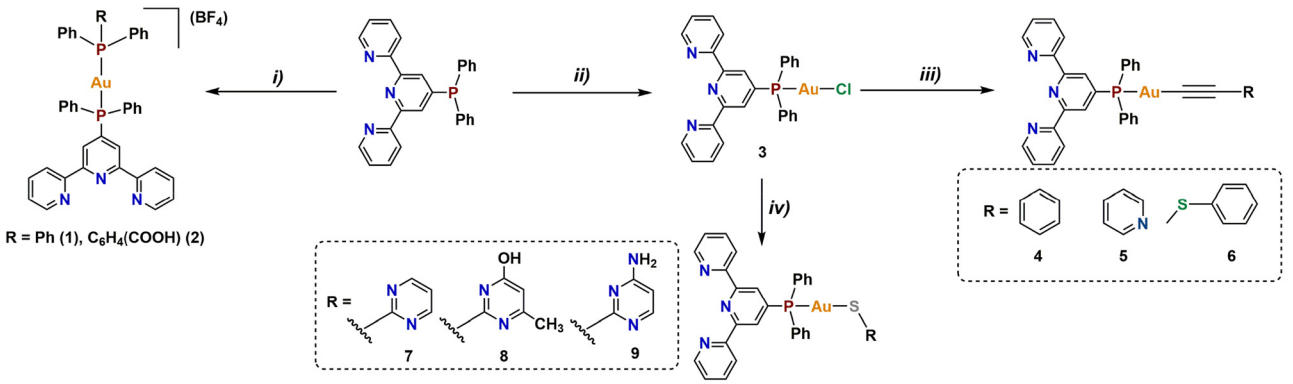

Scheme 1 Synthetic strategy to obtain gold complexes **1–9**. Experimental conditions: (i) AuCl[PPh_2R] + $AgBF_4$ in THF 2 h, (ii) AuCl(tht) in CH_2Cl_2 30 min, (iii) Alkyne + KOH in methanol 24 h, (iv) Thiol + Ag(acac) in CH_2Cl_2 12 h.

are neutral, and in each case, the protonated molecule has been identified (see Experimental section for more information).

Stability test

Stability studies were conducted using UV-visible spectroscopy. Compounds were dissolved in a mixture of PBS and DMF (10%), and the absorption spectra were recorded at various timeslots (t = 0, 24, 48, 72, and 96 h). The solution was maintained at 37 °C throughout the experiment, aligning with the temperature used for subsequent cytotoxicity assessments. Fig. 2 and Fig. S10–S17† demonstrate no discernible alterations in the absorption spectra, indicating the stability of all Au(I) compounds over the 96 h period. However, significant variations were observed after 24 h in the UV spectra of the free ligand. This may be due to the oxidation of phosphine (Fig. S18†).

Cytotoxicity and cellular uptake studies

Cytotoxicity studies. The cytotoxicity of gold complexes was evaluated *in vitro* against three human tumor cell lines: HT-29 (colorectal adenocarcinoma), MCF-7 (breast cancer), and MDA-MB-231 (triple-negative breast cancer) and healthy cells (primary fibroblast extracted from mouse ears). Cells were exposed to each compound for 72 h (HT-29 and primary fibroblast) or 96 h (MCF-7 and MDA-MB-231).

Cell viability was assessed using the crystal violet method for tumorigenic cell lines and MTT for primary fibroblasts, and IC_{50} values were determined from dose–response curves generated *via* nonlinear regression analysis, as summarised in Table 1.

All Au(I) derivatives exhibited potent cytotoxicity, with IC_{50} values below 0.5 μM across all tested tumor cell lines. Notably, variations in ancillary ligands did not significantly affect the cytotoxicity of these derivatives, even, the free 4′-PPh_2-terpy ligand demonstrated comparable activity; however, distinctions were observed among the different cell lines, with MDA-MB-231 showing the highest sensitivity with IC_{50} values close to 0.2 μM. In contrast, HT-29 and MCF-7 cell lines exhibited IC_{50} values approximately twice those of MDA-MB-231, nearing 0.4 μM.

These results are highly promising, as the Au(I) complexes surpassed the cytotoxicity observed with auranofin in the same cell lines, with IC_{50} values 10-fold lower. Moreover, the exceptional sensitivity of MDA-MB-231, representative of triple-negative breast cancer—a particularly aggressive subtype lacking hormone receptors—underscores the significance of these findings. To study healthy cells, fibroblasts were extracted from mouse ears and cultured to develop a primary culture that provided a source of healthy cells. The results shown in Table 1 indicate that the selected gold complexes exhibit certain selectivity, being about ten times more active against tumor cells compared to healthy cells, with a selectivity index (SI) ranging from 4 to 24. Among the compounds, those containing the phosphine group showed the lowest SI, while those with the thiolate group were the most selective. Interestingly, the free ligand demonstrated a higher SI than the gold complexes. Despite the moderate selectivity of the Au compounds against healthy cells, these results are promising, particularly given their high activity against various cancer cell lines and

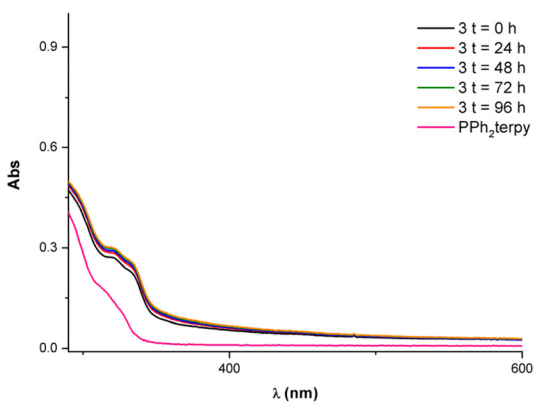

Fig. 2 Stability study of **3** and comparison with the ligand 4′-PPh_2terpy in a mixture of PBS/DMF (10%).

Table 1 IC_{50} values and experimental errors (±) of 4′-PPh_2terpy, **1** to **9** and auranofin as a reference in μM

		IC_{50} HT-29	IC_{50} MCF-7	IC_{50} MDA-MB-231	IC_{50} primary fibroblasts	SI
	A[a]	3.79 ± 0.18	2.00 ± 0.05	1.54 ± 0.12	n.d.	
	L[a]	0.37 ± 0.04	0.39 ± 0.05	0.24 ± 0.10	22.66 ± 0.69	58–94
Phosphines	1	0.40 ± 0.06	0.43 ± 0.11	0.27 ± 0.01	n.d.	n.d.
	2	0.38 ± 0.09	0.50 ± 0.14	0.27 ± 0.01	2.05 ± 0.30	4–8
Cl	3	0.41 ± 0.04	0.44 ± 0.08	0.25 ± 0.10	4.40 ± 0.64	10–17
Alkynyls	4	0.37 ± 0.07	0.38 ± 0.11	0.20 ± 0.03	2.78 ± 0.20	7–14
	5	0.45 ± 0.15	0.43 ± 0.04	0.28 ± 0.02	n.d.	n.d.
	6	0.43 ± 0.06	0.52 ± 0.05	0.31 ± 0.04	n.d.	n.d.
Thiolates	7	0.34 ± 0.05	0.28 ± 0.10	0.20 ± 0.06	4.85 ± 0.17	14–24
	8	0.42 ± 0.06	0.34 ± 0.09	0.26 ± 0.10	n.d.	
	9	0.40 ± 0.05	0.34 ± 0.14	0.23 ± 0.09	n.d.	

[a] A = auranofin, L = 4′-PPh_2terpy. Selectivity Index (SI) calculated as IC_{50} (Fibroblasts)/IC_{50} (tumour cell line).

their potential dual mechanism behaviour, with two main biological targets: DNA (targeted by terpyridine ligands)[10–12] and TrR (targeted by gold complexes).[2,4–8]

Cellular uptake studies. Compounds **3** and **4** were selected to evaluate the internalisation of gold inside the cell. For this purpose, the MDA-MB-231 cells were incubated in the presence of **3** and **4** at a concentration of 0.4 μM (157.57 ng of Au) during 48 h. The Au content was evaluated by ICP-MS, revealing 21.86 ± 1.07 and 24.80 ± 0.13 ng of Au in 6 10^4 cells. The percentage of internalisation was calculated for both **3** and **4**, showing that after 48 h of incubation, 14 and 15% of Au was internalised inside the cell, respectively.

Ligand exchange reactions with *N*-acetyl-L-cysteine

As mentioned above, the main mode of action of gold compounds is the interaction with thiols present in proteins such as albumin, immunoglobulins, and enzymes like TrxR. Gold is able to coordinate through ligand exchange reactions with cysteine and selenocysteine residues present in the active sites of these enzymes, inhibiting them.[2,4–8] Therefore, the ligand exchange ability of complexes **2** (phosphine), **3** (chloride), **4** (alkynyl) and **7** (thiolate) in presence of *N*-acetyl-L-cysteine (NAC) was evaluated and different results were observed depending on the ancillary ligand used. To evaluate these ligand exchange reactions, ^1H and $^{31}P\{^1H\}$ NMR studies were carried out at different times. Thus, upon the addition of one equivalent of NAC to a 10 mM solution of complex **2**, an immediate reaction ensued, leading to an equilibrium between the phosphine ligand and NAC, as shown by ^1H and $^{31}P\{^1H\}$ NMR spectra (see ESI Fig. S19†). After 90 min, a small amount of phosphine oxide is also observed, likely due to of a slow exchange between the phosphine ligand and NAC. For compound **3**, the exchange between the chloride ligand and the NAC was instantaneous. Once NAC was coordinated, no exchange equilibrium was established, as evidenced by both the ^1H NMR spectra (see Fig. S20†) and the defined signals observed in the $^{31}P\{^1H\}$ NMR spectra (Fig. 3). Regarding **4**, whit an alkynyl as ancillary ligand, a slow exchange between the phenylacetylene ligand and NAC was observed. In ^1H NMR spectrum (Fig. S21† up) showed that after 20 minutes, the signal of the terminal CH corresponding to the alkyne

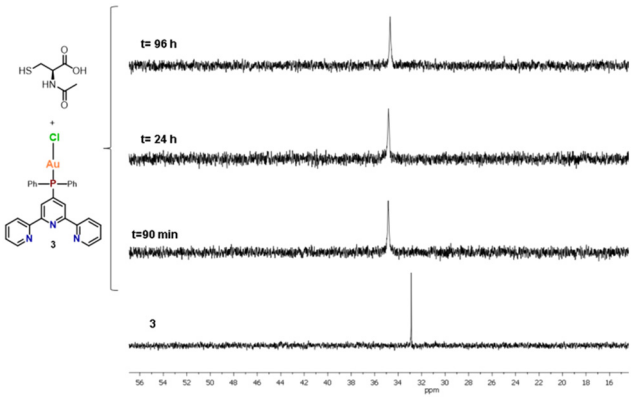

Fig. 3 $^{31}P\{^1H\}$ NMR (DMSO) of complex **3** (10 mM) in presence of 1 equivalent of NAC.

increased. Furthermore, the $^{31}P\{^1H\}$ NMR spectrum indicated an equilibrium between the phenylacetylene group and NAC, with a small amount of phosphine oxide also observed (Fig. S21† bottom). For complex **7**, where the ancillary ligand is a thiolate, the ligand exchange reaction is immediate, and an equilibrium is established between the different thiolates, as shown in the $^{31}P\{^1H\}$ NMR spectrum where broad signals can be observed (Fig. S22†). This ligand exchange study establishes a correlation between the leaving group capacities of different ligands and the speed of ligand exchange reactions, following the order: alkynyl < phosphine < thiolate < chloride.

DNA binding studies

UV-vis titration experiments. The absorption spectral titration experiments were conducted following the methodology outlined in our prior work.[10] For DNA binding studies, we selected complexes **2**, **3**, **4** and **7**, along with the ligand 4′-PPh_2terpy. These compounds were chosen to represent a diverse sample of the synthesised gold complexes, while the inclusion of the ligand 4′-PPh_2terpy was based on its comparable cytotoxicity. In Fig. 4, the UV-vis spectra obtained by gradually adding increasing amounts of DNA to a solution of **3** are depicted (see Fig. S23–S27 in ESI†), while Table 2 presents the data extracted from the absorption spectral titration experiments.

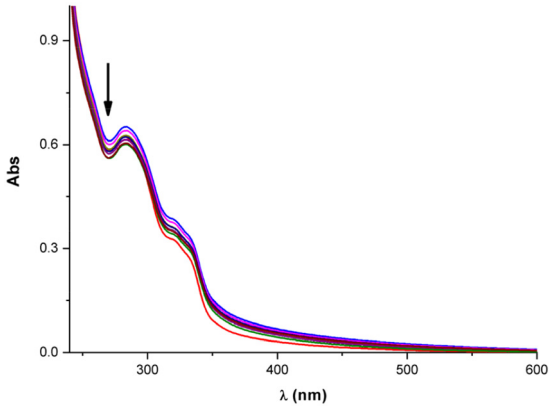

Fig. 4 Absorption spectral titration experiment for complex **3**. The arrow indicates that the absorbance of the complex decreases with the addition of CT-DNA.

Table 2 DNA binding constants

	λ_{study}(nm)	Bathochromism (nm)	K_b (M^{-1})
L[a]	260	—	5.09×10^4
2	260	—	7.64×10^4
3	284	2	5.70×10^4
4	250	—	1.01×10^7
7	256	3	2.08×10^4

[a] L = 4′-PPh_2terpy.

In all the spectra, a decrease in the intensity of the band across the entire wavelength range is observed, with some cases displaying a slight red shift (2–3 nm), suggesting potential interaction of the complexes with DNA through intercalation. When the complex interacts with DNA *via* intercalation, presumably through weak interactions between the ligand and the DNA base pairs, a combination of π electrons from the compound and the π electrons of the DNA nitrogenous bases leads to a decrease in the energy of the electronic π–π* transition, resulting in bathochromism. Additionally, the partially occupied π orbital of the DNA base pairs diminishes the likelihood of the transition, causing hypochromism. Typically, when interaction with DNA occurs through intercalation, both hypochromism and bathochromism processes are present, though a pronounced red shift is not always evident.[21–23] With regard to the DNA-binding constant (K_b) for the 4′-PPh_2terpy ligand as well as for complexes **2**, **3** and **7**, all are within the 10^4 M^{-1} order, indicating a moderate interaction with DNA. The use of ancillary ligands such as phosphine, chloride, and thiolate does not appear to influence the mode of interaction with DNA, possibly because these complexes interact with DNA through the terpyridine moiety. In contrast, for **4**, K_b = 1.01×10^7 M^{-1}, indicating a three-fold higher interaction strength with DNA, placing it within the range of classical intercalating agents like ethidium bromide (EB K_b $1{,}4 \times 10^6$ M^{-1}) or others.[24,25] The key distinction between **4** and the preceding complexes lies in the planarity of the ancillary ligand used in this case (phenylacetylene). It is plausible that the increased planarity of **4** facilitates greater insertion between consecutive base pairs of the DNA double helix, thereby enhancing the number of interactions and, consequently, the strength of the DNA-complex interaction.

Competitive assay of fluorescence quenching. Ethidium bromide (EB) is a classical DNA intercalator. Upon intercalation with DNA, it forms a fluorescent complex. Therefore, to confirm that our complexes are intercalating agents, an EB quenching study was carried out. If the complexes are intercalating agents, they will be able to displace the EB, resulting in decreased fluorescence intensity. Compounds **3** and **4** have been selected, as they show differences in DNA binding constants (K_{b3} = 5.70×10^4, K_{b4} = 1.01×10^7). Fig. 5 shows the emission spectra of EB and DNA in the presence of increasing concentrations of **3** and **4**. As can be seen, compound **4** is able to displace more EB than compound **3** in the same concentration range. These results confirm that both compounds are intercalating agents and that complex **4** is a better intercalator than complex **3**.

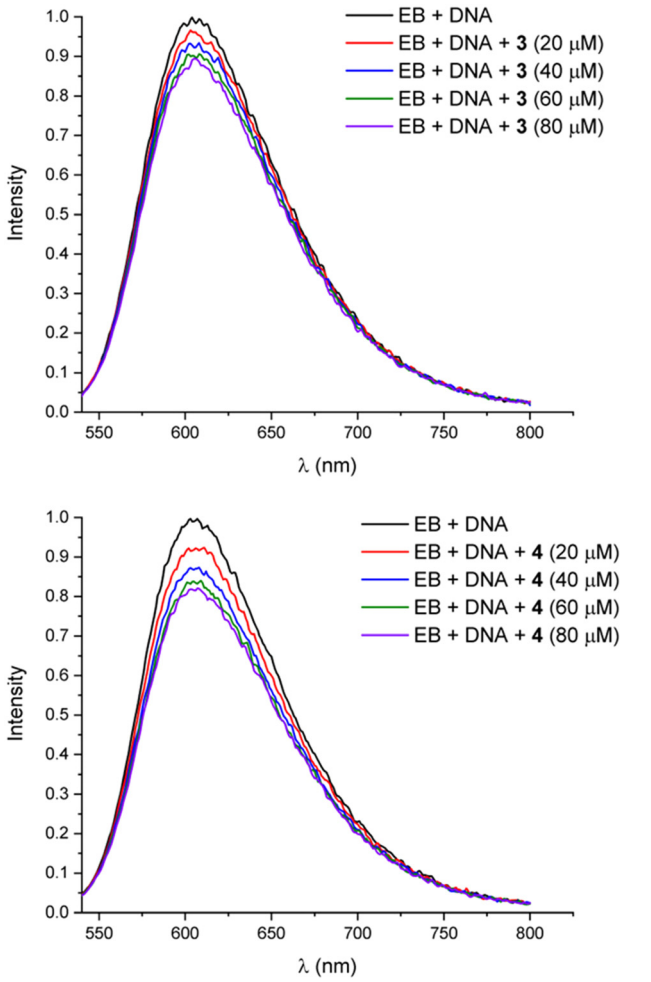

Fig. 5 Ethidium bromide quenching experiment in presence of complexes **3** and **4**.

Thioredoxin reductase inhibition studies

Several studies have indicated that the primary biological target of auranofin and other Au(I) compounds is thioredoxin reductase (TrxR).[9,26] For this reason, we selected the compounds **2**, **3**, **4** and **7**, as well as the ligand 4′-PPh_2terpy, to evaluate whether they were able to inhibit the activity of the isolated enzyme. The enzyme inhibition study of the 4′-PPh_2terpy ligand was carried out at 5 μM revealing an enzyme activity of 89% relative to the untreated control, suggesting negligible inhibition of TrxR function by the ligand.

In contrast, compounds **2**, **3**, **4** and **7** were studied at 10-fold lower concentration (0.5 μM), resulting in enzymatic activity of less than 50% in all cases (see Table 3). Notably, significant differences emerged among the complexes with different ancillary ligands, with the alkynyl functional group inducing the lowest inhibition, with an enzymatic activity of 39% (Table 3). This was followed by the phosphine group at 25%, while the chloride and thiolate functional groups exhibited the highest enzymatic inhibition, with enzymatic activities of 12% and 19%, respectively. Hence, a relationship between the ancillary ligand employed and the observed enzyme inhibition seems plausible, following the order alkynyl < phosphine < thiolate < chloride. This pattern aligns with the ability of the ancillary ligands to be replaced by the selenol groups of TrxR. Given that the chloride functional group yielded the most promising results, we exemplarily determined the IC_{50} value of **3**, which falls within the nanomolar range. This data confirms the potent inhibition exerted by **3** on the TrxR system, with a comparable value to auranofin (IC_{50} = 0.093 ± 0.009 μM), known for its high selectivity in TrxR inhibition.

Flow cytometry studies

Mechanism of cell death. One defining trait of cancer cells is the imbalance between cell division and cell death, with disease progression relying on the disruption of cell death pathways. Therefore, understanding how complexes trigger cell death is crucial. Compounds that activate programmed cell death pathways, such as apoptosis, rather than necrosis, which causes severe inflammation, are particularly important. The mechanism of cell death was analysed using flow cytometry by labeling cells with double staining with Annexin V-FITC and propidium iodide. Table 4 summarises the results for complexes **3** and **4** and the control (see Fig. S29†). The number of necrotic cells remained unchanged for both the control and the MDA-MB-231 cells incubated for 48 h with compounds **3** and **4**. However, the number of early and late apoptotic cells increased from 3.42% in the control to 20.03% with compound **3** and 17.52% with compound **4**. These results suggest that both compounds induce apoptosis.

Table 3 Enzyme activity in % (A_{TrxR}) and IC_{50} values

	A_{TrxR}% [*I*] = 5 μM	A_{TrxR}% [*I*] = 0.5 μM	$IC_{50\ TrxR}$ (μM)
L[a]	89 ± 10	n.d.	n.d.
A[a]	n.d.	n.d.	0.093 ± 0.009
2	n.d.	25.5 ± 0.8	n.d.
3	n.d.	12 ± 9	0.085 ± 0.029
4	n.d.	39 ± 16	n.d.
7	n.d.	19 ± 4	n.d.

[a] L = 4′-PPh_2terpy, A = auranofin.

Table 4 Percentage of intact, apoptotic or necrotic cells

	Intact cells	Early apoptotic cells	Late apoptotic cells	Necrotic cells
Control	96.24	1.08	2.34	0.33
3	79.57	5.12	14.91	0.41
4	81.97	5.38	12.14	0.50

Cell cycle arrest studies. Cell division is a regulated mechanism responsible for splitting a cell into two daughter cells. The cell cycle comprises two main phases: mitosis (M), where cell division occurs, and interphase, which includes the G1 (pre-DNA synthesis), S (DNA synthesis), and G2 (pre-division) stages. After interphase, the cell can enter the G0 phase (quiescence), describing cells not in the cell cycle but with the potential for division. G0 predominantly contains non-growing or non-proliferating cells. Cells transition from the quiescent G0 to G1 phase in response to proliferation signals or other mitogenic stimuli. Cell cycle progression is primarily controlled by two regulatory processes: phosphorylation of specific proteins by cyclin-dependent kinases (CDKs) and their dephosphorylation by phosphatases; and specific proteolytic degradation by the ubiquitin-proteasome system. The transitions from G1 to S and G2 to M are key points in the cell cycle and therefore there are so-called checkpoints. The aim of these checkpoints is to control the genome to ensure the viability of the daughter cells. Activation of p53 gene blocks the phase-transition proteins cyclins D and E for the G1-S transition and cyclin B for G2-M. Furthermore, p53 gene is closely related to apoptosis, which is why an arrest in the cell cycle often leads to a mechanism of death programme such as apoptosis.[27]

Studying the cell cycle can elucidate the mechanisms of action of potential drugs. Quantifying DNA content by flow cytometry allows for understanding the distribution of cell populations across different cell cycle phases. MDA-MB-231 cells were incubated with compounds **3** and **4** for 48 h. As shown in Table 5 and ESI Fig. S30,† the presence of compounds **3** and **4** significantly increased the number of cells in the G0/G1 phase and led to a corresponding decrease in the G2/M phase compared to the control. However, there was no significant effect on the S phase. These data suggest that G0/G1 phase arrest may be responsible for the anti-proliferative effects of compounds **3** and **4** on MDA-MB-231 cells.[28] Arrest

Table 5 Percentage of cells in the different phases of cell cycle

	G0G1	S-Phase	G2M
Control	56.68	29.04	14.28
3	69.77	24.83	5.41
4	70.24	24.86	4.90

in the G0/G1 phase can result from severe and irreparable DNA damage, preventing the cell from entering the S phase. Literature reports indicate that DNA intercalating agents and ROS production can induce G0/G1 arrest.[29]

ROS production studies. Redox homeostasis plays an essential role in the maintenance of various cellular processes. Disruption of redox homeostasis leads to an increase in reactive oxygen species (ROS) that can trigger damage to proteins and or DNA and can cause cell death by oxidative stress.[30] Furthermore, the production of ROS tends to produce a programmed death such as apoptosis or autophagy. Therefore, the ability of compounds **3** and **4** to induce ROS in MDA-MB-231 cells was evaluated. ROS production can be detected by flow cytometry using fluorogenic sensors which in their reduced form are not fluorescent, but in their oxidised form shows an intense fluorescence. Fig. 6 shows a considerable increase in fluorescence intensity in the presence of compounds **3** and **4** with respect to the control, indicating an increase in ROS production in the presence of the complexes studied.

Mitochondrial potential. The mitochondrion is an organelle that controls both lethal and vital functions of the cell. As a critical centre of metabolic activities and implicated in many diseases, mitochondria have attracted attention as a potential therapeutic target, especially for the treatment of cancer. Changes in mitochondrial membrane potential indicate mitochondrial damage. The membrane potential ($\Delta\Psi$) is generated and maintained by ion concentration gradients. The mitochondrial $\Delta\Psi$ is reduced when energy metabolism is interrupted.[31] Flow cytometry can be used to estimate the mitochondrial membrane potential using cyanine dyes that can detect changes in the $\Delta\Psi$, due to the fact that the mean fluorescence intensity decreases when the mitochondrial $\Delta\Psi$ is altered. After incubation of MDA-MB-231 cells in the presence of compounds **3** and **4** during 48 h, it was possible to observe an increase in the number of cells showing a decrease in mitochondrial $\Delta\Psi$ as shown in Fig. S31.† Thus, while in the control 92.01% of the cells showed a normal mitochondrial membrane potential, in the presence of **3** and **4** these were reduced to 68.09% and 61.50% respectively. These results demonstrate that both complex **3** and **4** were able to decrease the mitochondrial membrane potential.

Flow cytometry studies have concluded that after 48 h of incubation with selected compounds **3** and **4**, MDA-MB-231 cells underwent apoptosis, experienced cell cycle arrest in the G0/G1 phase, showed increased ROS levels, and had reduced mitochondrial potential.

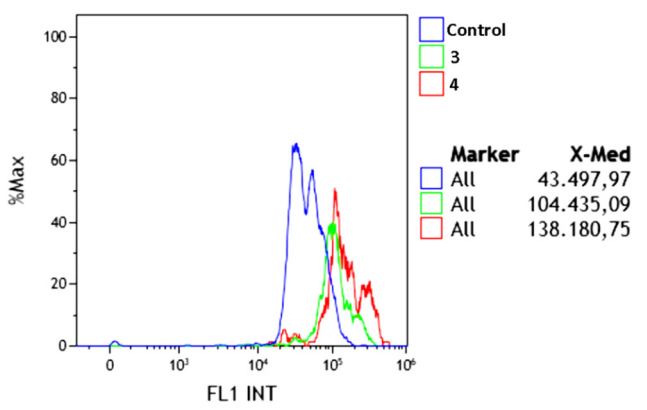

Fig. 6 Histograms of ROS production (blue: control, green: **3** and red: **4**).

Conclusions

In this study, we have successfully synthesised various Au(I) derivatives employing the 4′-PPh$_2$terpy ligand, represented by the general formula [Au(L)(4′-PPh$_2$terpy)]$^{0/+1}$. The utilisation of this ligand ensures the stability of Au(I) compounds with terpyridine-derived ligands in solution, enabling a comprehensive examination of their properties as potential anticancer agents.

Our investigation into the antitumor properties of these derivatives has yielded promising results, as all compounds demonstrated high activity against different tumor cell lines, including HT-29 (colorectal adenocarcinoma), MCF-7 (breast cancer), and MDA-MB-231 (triple-negative breast cancer). While minimal variations were observed among the different Au(I) compounds (**1–9**), distinctions emerged in their activities against the various cell lines. Notably, the most significant efficacy was observed against the MDA-MB-231 cell line, with IC_{50} values approximately half of those observed for HT-29 and MCF-7 (IC_{50} MDA-MB-231 $\approx$ 0.2 μM; IC_{50} HT-29/MCF-7 $\approx$ 0.4 μM). Importantly, compounds **1–9** exhibited superior results compared to auranofin, with IC_{50} values approximately tenfold lower. Particularly noteworthy is the exceptional efficacy against triple-negative breast cancer (MDA-MB-231), one of the most aggressive forms of breast cancer. In addition, our studies can conclude that, our complexes show certain selectivity towards healthy fibroblasts, with a selectivity index of 24 in the best case.

Moreover, considering that gold complexes typically interact with thiol groups present in different biomolecules, the capability of different ancillary ligands to engage in ligand exchange reactions with thiol groups, such as NAC, has been examined using ^{1}H and ^{31}P{^{1}H} NMR. This evaluation unveiled a correlation between the leaving group capacities of various ligands and the speed of ligand exchange reactions, with the order being alkynyl < phosphine < thiolate < chloride.

Furthermore, our efforts to elucidate potential biological targets and mechanisms of action revealed that representative Au(I) derivatives (**2**, **3**, **4**, and **7**) and the ligand 4′-PPh$_2$terpy interact *via* an intercalation mechanism with DNA. The calculation of the DNA-binding constant (K_b) indicated moderate interaction for the ligand and **2**, **3**, and **7**, with K_b values in the range of 10^{-4} M^{-1}, likely attributed to their interaction with DNA through the terpyridine moiety. In contrast, **4** exhibited a strong interaction with DNA (K_b = 1.01 × 10^7 M^{-1}), possibly due to its enhanced planarity resulting from the use of the

ancillary ligand phenylacetylene, leading to increased insertion between DNA strands.

Moreover, our investigation into the enzymatic inhibition of the TrxR system unveiled compelling findings. While the ligand itself exhibited minimal activity, intriguing variations were observed in the gold complexes among the different ancillary ligands (phosphine, chloride, alkynyl, or thiolate). A direct correlation was noted between the observed inhibition and the ability of the ancillary ligand to exchange with the selenol groups of TrxR, consistent with findings from ligand exchange studies. The chloride functional group yielded the most promising results (as evidenced by **3**), displaying inhibition levels similar to auranofin in the nanomolar range.

Flow cytometry studies suggest that the synthesised Au(I) complexes with terpyridine ligands exhibit a dual mechanism involving DNA interaction and inhibition of the TrxR system. This is indicated by G0/G1 phase arrest, implying DNA damage that prevents progression to the S-phase. This may result from both DNA intercalation and oxidative stress due to TrxR inhibition.[28,32] The G0/G1 arrest is commonly associated with apoptosis,[27] explaining the cell death induced by these compounds. Since the TrxR system is crucial for cellular antioxidant defense, its inhibition leads to increased oxidative stress, evidenced by higher ROS levels and reduced mitochondrial membrane potential.

Collectively, these findings underscore the feasibility of synthesising stable gold(I) complexes with terpyridine-derived ligands and highlight both DNA and TrxR as potential biological targets for these compounds. Consequently, our results reaffirm the significant potential of these derivatives as promising anticancer agents.

Experimental section

Instruments and general information

Fourier transform infrared (FT-IR) spectra were recorded in the 4000–450 cm^{-1} range on a PerkinElmer μ-ATR Spectrum II. C, H, and N analyses were carried out with PerkinElmer 240C microanalyser. Mass spectra were carried out with Bruker microTOF-Q hybrid quadrupole-time-of-flight mass spectrometer with ESI ionisation. ^1H and $^{31}P\{^1H\}$ NMR spectra were recorded with a Bruker Avance 400 or 300 spectrometer. Absorption spectra in solution were recorded on a Hewlett–Packard 8453 diode array UV–Vis spectrophotometer.

Materials and procedures. The starting materials used in this work have been purchased from Alfa Aesar or Sigma Aldrich and used as received.

Synthesis of the compounds

Synthesis of 4′-PPh_2terpy. The existing protocol in the literature[33] has been modified: a suspension in CH_3CN (deoxygenated, 40 mL) of KOH (2 g) and K_2CO_3 (5.5 g) is stirred under reflux conditions under inert atmosphere for 1 h. Then diphenylphosphine (PPh_2H) (750 μL 3.7 mmol) is added, the solution turns orange due to the formation of the $[PPh_2]^-$ anion, after 1 h under reflux 1 equivalent of 4′-Clterpy ligand (1 g, 3.7 mmol) is added and left to react for 15 min. The solution progressively loses its colour until a colourless solution is obtained. Finally, the reaction is allowed to reach room temperature and the reaction is poured over 80 ml of water. Immediately, a white solid appears. Yield 80%. ^1H NMR (400 MHz, d_6-$(CH_3)_2O$, ppm): δ 8.71 (m, 2H, H4), 8.60 (m, 2H, H1), 8.45 (d, 2H, H5, $^3J_{P-H}$ = 7,10 Hz), 7.97 (ddd, 2H, H3, $^3J_{H3-H2} \sim {}^3J_{H3-H4}$ = 7.73 Hz, $^4J_{H3-H1}$ = 1.80 Hz), 7.49 (m, 10H, Ph), 7.42 (ddd, 2H, H2, $^3J_{H2-H3}$ = 7.50 Hz, $^3J_{H2-H1}$ = 4.81 Hz, $^4J_{H2-H4}$ = 1.17 Hz). $^{31}P\{^1H\}$ NMR (162 MHz, d_6-$(CH_3)_2O$, ppm): δ −5.10.

*Synthesis of [Au(PPh_2R)(4′-PPh_2terpy)]BF_4 (R = Ph (**1**), C_6H_4COOH (**2**)).* A solution of [AuCl(PPh_3)]/[AuCl(PPh_2(C_6H_4COOH))] (0.1592 g, 0.32 mmol/0.1724 g, 0.32 mmol) in anhydrous THF (20 mL) is prepared under inert atmosphere, allowing the solution to cool in ice bath for 30 min. Then, 1 equivalent of $AgBF_4$ (0.0622 g, 0.32 mmol) is added and a white precipitate (AgCl) immediately appears, adding the 4′-PPh_2terpy ligand (0.1336 g, 0.32 mmol) and stirring the mixture for 2 h (protected from light). Then, the solution was filtered over Celite and active carbon, and the volume reduced under vacuum. The complexes **1** and **2** were precipitated with diethyl ether.

*[Au(PPh_3)(4′-PPh_2terpy)]BF_4 (**1**).* White solid, yield = 73%. ^1H NMR (400 MHz, d_6-$(CH_3)_2O$, ppm): δ 8.69 (m, 4H, H4 + H5), 8.59 (m, 2H, H1), 7.99 (m, 2H, H3), 7.91–7.64 (m, 25H, Ph) 7.46 (m, 2H, H2). $^{31}P\{^1H\}$ NMR (162 MHz, d_6-$(CH_3)_2O$, ppm): δ 43.80 (m, 2P, PPh_2 + PPh_3). ESI(−) (acetone) *m*/*z* = $[BF_4]^-$ 87, ESI (+) exact mass *m*/*z*: $[Au(PPh_3)(4'\text{-}PPh_2terpy)]^+$ calculated = 876.1966, found = 876.1957; $[Au(PPh_3)_2]^+$ calculated = 721.1488, found = 721.1559; $[Au(4'\text{-}PPh_2terpy)_2]^+$ calculated = 1031.2455, found = 1031.2403. FT-IR(ATR): ν(C═N) a 1560 cm^{-1}; ν(C═C) 1474 cm^{-1}; $\nu(C^{Ar}\text{–H})$ a 1056 cm^{-1}, ν(P–C) 690 cm^{-1}. Analytical data (%): $C_{45}H_{35}AuBF_4N_3P_2$ (963.50) requires C 56.09, H 3.66, N 4.36; found: C 56.34; H 3.81, N 4.09.

*[Au(PPh_2(C_6H_4COOH))(4′-PPh_2terpy)]BF_4 (**2**).* White solid, yield = 75%. ^1H NMR (400 MHz, d_6-$(CH_3)_2O$, ppm): δ 8.57 (m, 4H, H4 + H5), 8.51 (m, 2H, H1), 8.09 (d, 2H, HA, $^3J_{HA-HB}$ = 8.23 Hz), 7.92 (m, 2H, H3), 7.74–7.55 (m, 22H, Ph) 7.39 (m, 2H, H2). $^{31}P\{^1H\}$ NMR (162 MHz, d_6-$(CH_3)_2O$, ppm): δ 42.59 (m, 1P, PPh_2) 41.72 (m, 1P, $PPh_2C_6H_4COOH$). ESI (−) (acetone) *m*/*z* = $[BF_4]^-$ 87, ESI (+) exact mass *m*/*z*: $[Au(PPh_2C_6H_4COOH)(4'\text{-}PPh_2terpy)]^+$ calculated = 920.1865, found 920.1868, $[Au(PPh_2C_6H_4COOH)_2]^+$ calculated = 809.1285, found = 809.1277; $[Au(4'\text{-}PPh_2terpy)_2]^+$ calculated = 1031.2455, found = 1031.2460. FT-IR(ATR): ν(C═O) a 1706 cm^{-1}; ν(C═N) 1564 cm^{-1}; ν(C═C) a 1440 cm^{-1}; ν(C–O) a 1263 cm^{-1} $\nu(C^{Ar}\text{–H})$ a 1056 cm^{-1}, ν(P–C) a 690 cm^{-1}. Analytical data (%): $C_{46}H_{35}AuBF_4N_3O_2P_2$ (1007.50) requires C 54.84, H 3.50, N 4.17; found: C 54.62; H 3.78, N 4.36.

*Synthesis of [AuCl(4′-PPh_2terpy)] (**3**).* To a solution of [AuCl(tht)] (0.1038 g 0.3 mmol) in CH_2Cl_2 (20 ml) was added 1 equivalent of 4′-PPh_2terpy (0.1351 g 0.3 mmol). The mixture was stirred during 30 min and the volume reduced under vacuum.

The complex **3** was precipitated with *n*-hexane as a white solid. Yield 83%. ^{1}H NMR (400 MHz, d_6-$(CH_3)_2O$, ppm): δ 8.74 (m, 2H, H4), 8.66 (d, 2H, H5, J_{H-P} = 13.20 Hz), 8.64 (m, 2H, H1), 8.01 (ddd, 2H, H3, $^3J_{H3-H2} \sim {}^3J_{H3-H4}$ = 7.64 Hz, $^4J_{H3-H1}$ = 1.73 Hz), 7.86–7.68 (m, 10H, Ph), 7.48 (ddd, 2H, H2, $^3J_{H2-H3}$ = 7.59 Hz, $^3J_{H2-H1}$ = 5.92 Hz, $^4J_{H2-H4}$ = 1.20 Hz). $^{31}P\{^1H\}$ NMR (162 MHz, d_6-$(CH_3)_2O$, ppm): δ 33.28 (s, 1P). ESI (+) exact mass (acetone) *m*/*z*: $[AuCl(4'\text{-}PPh_2terpy)H]^+$ calculated = 650.0822 found = 650.0818. FT-IR(ATR): ν(C═N) 1551 cm^{-1}; ν(C═C) a 1461 cm^{-1}, $\nu(C^{Ar}\text{–}H)$ a 1092 cm^{-1}. Analytical data (%): $C_{27}H_{20}AuClN_3P$ (649.86) requires C 49.90, H 3.10, N 6.47; found: C 49.74; H 3.33, N 6.76.

*Synthesis of [Au(C≡CR)(4′-PPh$_2$terpy)] (R = Ph (**4**), 2-py (**5**), CH$_2$SPh (**6**)).* In a saturated solution of KOH in MeOH (5 mL) was added the corresponding alkyne phenylacetylene: 34.4 μL (0.31 mmol), 2-ethynylpyridine: 46.46 μL (0.46 mmol), phenylpropargyl sulphide 63.31 μL (0.46 mmol) and 1 equivalent of complex **3**. Immediately a yellow precipitate begins to appear in all cases. After 24 h the solids are filtered off and the solids washed with water (10 mL × 3).

*[Au(C≡CPh)(4′-PPh$_2$terpy)] (**4**).* Yellow solid, yield 67%. ^{1}H NMR (400 MHz, CD_2Cl_2, ppm): δ 8.64 (m, 4H, H4 + H1), 8.58 (d, 2H, H5, J_{H-P} = 13.26 Hz), 7.90 (ddd, 2H, H3, $^3J_{H3-H2} \sim {}^3J_{H3-H4}$ = 7.53 Hz, $^4J_{H3-H1}$ = 1.77 Hz), 7.75–7.21 (m, 17H, Ph + H2 + H_{Ar}). $^{31}P\{^1H\}$ NMR (162 MHz, CD_2Cl_2, ppm) δ 42.17 (s, 1P). ESI (+) exact mass (acetone) *m*/*z*: $[Au(Ph{\equiv})(4'\text{-}PPh_2terpy)H]^+$ calculated = 716.1524, found = 716.1516. FT-IR(ATR): ν(C≡C) 2118 cm^{-1}, ν(C═N) 1564 cm^{-1}; ν(C═C) 1470 cm^{-1}, $\nu(C^{Ar}\text{–}H)$ 1101 cm^{-1}. Analytical data (%): $C_{35}H_{25}AuN_3P$ (715.53) requires C 58.75, H 3.52, N 5.87; found: C 58.99; H 3.23, N 6.76.

*[Au(C≡CPy)(4′-PPh$_2$terpy)] (**5**).* Yellow solid, yield 62%. ^{1}H NMR (400 MHz, CD_2Cl_2, ppm): δ 8.66 (m, 4H, H4 + H1), 8.59 (d, 2H, H5, J_{H-P} = 13.44 Hz), 8.59 (m, 1H, HA) 7.90 (ddd, 2H, H3, $^3J_{H3-H2} \sim {}^3J_{H3-H4}$ = 7.57 Hz, $^4J_{H3-H1}$ = 1.74 Hz), 7.76–7.56 (m, 17H, Ph + HD), 7.35 (m, 3H, H2 + HC), 7.71 (m, 1H, HB). $^{31}P\{^1H\}$ NMR (162 MHz, CD_2Cl_2, ppm) δ 42.24 (s, 1P). ESI (+) exact mass (acetone) *m*/*z*: $[Au(PyC{\equiv}C)(4'\text{-}PPh_2terpy)H]^+$ calculated = 717.1477, found = 717.1460. FT-IR(ATR): ν(C≡C) 2121 cm^{-1}, ν(C═N) 1560 cm^{-1}; ν(C═C) 1451 cm^{-1}, $\nu(C^{Ar}\text{–}H)$ 1101 cm^{-1}. Analytical data (%): $C_{34}H_{24}AuN_4P$ (716.52) requires C 56.99, H 3.38, N 7.82; found: C 56.74, H 3.47, N 7.99.

*[Au(C≡CCH$_2$SPh)(4′-PPh$_2$terpy)] (**6**).* Yellow solid, yield 60%. ^{1}H NMR (400 MHz, CD_2Cl_2, ppm): δ 8.64 (m, 4H, H4 + H1), 8.54 (d, 2H, H5, J_{H-P} = 13.16 Hz), 7.89 (ddd, 2H, H3, $^3J_{H3-H2} \sim {}^3J_{H3-H4}$ = 7.49 Hz, $^4J_{H3-H1}$ = 1.74 Hz), 7.70–7.17 (m, 17H, Ph + HB + H_{Ar}). $^{31}P\{^1H\}$ NMR (162 MHz, CD_2Cl_2, ppm) δ 41.61 (s, 1P). ESI (+) exact mass (acetone) *m*/*z*: $[Au(PhS(CH_2)C{\equiv}C)(4'\text{-}PPh_2terpy)H]^+$ calculated = 762.1402, found = 762.1405. FT-IR (ATR): ν(C≡C) 2124 cm^{-1}, ν(C═N) 1560 cm^{-1}; ν(C═C) 1470 cm^{-1}, $\nu(C^{Ar}\text{–}H)$ 1099 cm^{-1}. Analytical data (%): $C_{36}H_{27}AuN_3PS$ (761.62) requires C 56.77, H 3.57, N 5.52, S 4.21; found: C 56.97; H 3.82, N 5.74, S 4.46.

*Synthesis of [Au(SR)(4′-PPh$_2$terpy)] (R = pyrimidine (7), 6-methyl-thiouracil (**8**), 2-thiocytosine (**9**)).* To a solution of silver acetylacetonate (0.2768 g 0.91 mmol) in CH_2Cl_2 (20 ml) the corresponding thiol (2-mercaptopyrimidine: 0.0852 g (0.76 mmol), 6-methyl-thiouracil (0.0370 g, 0.26 mmol), or 2-thiocytosine (0.0331 g, 0.26 mmol) 9) and 1 equivalent of **3** were added. The reaction was stirred during 12 h and filtrated over Celite. The reduction of the volume under vacuum and addition of *n*-hexane yield complexes **7–9** as white solids

[Au(SPyrim)(4′-PPh$_2$terpy)] (7). white solid, yield 73%. ^{1}H NMR (400 MHz, $CDCl_3$, ppm): δ 8.65 (m, 6H, H4 + H1 + H5), 8.36 (d, 2H, HA, $^3J_{HA-HB}$ = 4.84 Hz), 7.86–7.55 (m, 12H, H3 + Ph), 7.34 (ddd, 2H, H2, $^3J_{H2-H3}$ = 7.30 $^3J_{H2-H1}$ = 4.75 Hz, $^4J_{H2-H4}$ = 0.96 Hz), 6.83 (t, 1H, HB, $^3J_{HB-HA,\ HB-HA'}$ = 4.88 Hz). $^{31}P\{^1H\}$ NMR (162 MHz, $CDCl_3$, ppm) δ 38.19 (s, 1P). ESI (+) exact mass (acetone) *m*/*z*: $[Au(S\text{–}pyrim)(4'\text{-}PPh_2terpy)H]^+$ calculated = 726.1150 found = 726.1171. FT-IR(ATR): ν(C═N) 1556 cm^{-1}; ν(C═C) 1482 cm^{-1}; $\nu(C^{Ar}\text{–}H)$ 1100 cm^{-1}. Analytical data (%): $C_{31}H_{23}AuN_5PS$ (725.55) requires: C 51.32, H 3.19, N 9.65, S 4.42; found: C 51.56, H 3.34, N 9.41, S 4.21.

*[Au(6–CH$_3$–2–SUra)(4′-PPh$_2$terpy)] (**8**).* white solid, yield 75%. ^{1}H NMR (400 MHz, $CDCl_3$, ppm): δ 9.82 (s, 1H, OH) 8.61 (m, 6H, H4 + H1 + H5), 7.86 (ddd, 2H, H3, $^3J_{H3-H2} \sim {}^3J_{H3-H4}$ = 7.53 Hz, $^4J_{H3-H1}$ = 1.90 Hz), 7.76–7.55 (m, 10H, Ph), 7.34 (ddd, 2H, H2, $^3J_{H2-H3}$ = 7.61 $^3J_{H2-H1}$ = 5.03 Hz, $^4J_{H2-H4}$ = 1.32 Hz), 5.89 (s, 1H, HA). $^{31}P\{^1H\}$ NMR (162 MHz, $CDCl_3$, ppm) δ 37.83 (s, 1P). ESI (+) exact mass (acetone) *m*/*z*: $[Au(6\text{–}CH_3\text{–}2\text{–}SUra)(4'\text{-}PPh_2terpy)H]^+$ calculated = 756.1256 found = 756.1269. FT-IR (ATR): ν(Ar–O–H) 3663 cm^{-1} ν(C═N) 1576 cm^{-1}; ν(C═C) 1474 cm^{-1}; $\nu(C^{Ar}\text{–}H)$ 1040 cm^{-1}. Analytical data (%): $C_{32}H_{25}AuN_5OPS$ (755.58) requires: C 50.87, H 3.33, N 9.27, S 4.24; found: C 50.99, H 3.06, N 9.46, S 4.41.

*[Au(2-SCyt)(4′-PPh$_2$terpy)] (**9**).* White solid, yield 75%. ^{1}H NMR (400 MHz, $CDCl_3$, ppm): δ 8.64 (m, 6H, H4 + H1 + H5), 7.91 (d, 1H, HB, $^3J_{HB-HA}$ = 5.85 Hz), 7.85 (ddd, 2H, H3, $^3J_{H3-H2} \sim {}^3J_{H3-H4}$ = 7.57 Hz, $^4J_{H3-H1}$ = 1.76 Hz), 7.76–7.52 (m, 10H, Ph), 7.52 (ddd, 2H, H2, $^3J_{H2-H3}$ = 7.71 $^3J_{H2-H1}$ = 5.12 Hz, $^4J_{H2-H4}$ = 1.52 Hz), 6.02 (d, 1H, HA, $^3J_{HA-HB}$ = 5.62 Hz), 4.91 (s, 2H, NH_2). $^{31}P\{^1H\}$ NMR (162 MHz, CD_1Cl_3, ppm) δ 37.70 (s, 1P). ESI (+) exact mass (acetone) *m*/*z*: $[Au(2\text{-}SCyt)(4'\text{-}PPh_2terpy)H]^+$ calculated = 741.1259, found = 741.1257. FT-IR(ATR): $\nu(NH_2)$ 3443–3333 cm^{-1}; ν(C═N) 1575 cm^{-1}; ν(C═C) 1462 cm^{-1}; $\nu(C^{Ar}\text{–}H)$ 1070 cm^{-1}. Analytical data (%): $C_{31}H_{24}AuN_6PS$ (740.57) requires: C 50.28, H 3.26, N 11.35, S 4.33; found C 50.47; H 3.01, N 11.51, S 4.46.

Ligand exchange studies

The NMR studies were carried out in a Bruker Avance 300 in d_6-DMSO. The experiments were performed at a concentration of 10 mM of complex **2**, **3**, **4**, **7** or ligand in presence of 1 equivalent of *N*-acetyl-L-cysteine (NAC). The spectra were recorded at different time points. ^{1}H NMR every 10 minutes during the first 90 minutes and after 24 and 96 h. $^{31}P\{^1H\}$ NMR after 90 min, 24 and 96 h.

Cell culture tumour cell lines

HT-29 colon carcinoma cells, MDA-MB-231 breast cancer cells, and MCF-7 breast carcinoma cells were maintained in Dulbecco's modified Eagle's medium (DMEM; 4.5 gL^{-1}

D-glucose, L-glutamine, pyruvate), supplemented with gentamycin (50 mgL^{-1}) and fetal bovine serum superior, standardised (Biochrom GmbH, Berlin) (10% v/v), with a weekly passage.

Antiproliferative assay

The antiproliferative effects were determined according to a recently used method with minor modifications.[34,35] Briefly, 100 mL of HT-29 cells (2565 cells per mL), MDA-MB-231 cells (4120 cells per mL) or MCF-7 cells (4840 cells per mL) was transferred into the wells of 96-well plates and incubated at 37 °C under 5% CO_2 for 96 h (MCF-7, MDA-MB-231, RC-124) or 72 h (HT-29). Stock solutions of the compounds in dimethylformamide (DMF) were freshly prepared and diluted with the respective cell culture medium to graded concentrations (final concentration of DMF: 0.1% v/v). After 72 h (HT-29) or 96 h (MCF-7, MDA-MB-231) of exposure, the cell biomass was determined by crystal violet staining, and the IC_{50} value was determined as the concentration that caused 50% inhibition of cell proliferation compared to an untreated control. Results were calculated as the mean values of three independent experiments.

Extract healthy fibroblasts from mouse ears and preparation of the primary culture

Primary cells are obtained from living tissue and cultured *under in vitro* conditions. The mouses were housed in a pathogen-free environment according to European Union guidelines until euthanasia. The protocol established by Stephan Gasser was followed, with minor modifications.[36]

Digestion solution. Gey's buffer 1.5 mg mL^{-1} Collagenase I (Gibco 17100-017). Culture medium: Dulbecco's modified Eagle's medium (DMEM; 4.5 gL^{-1} D-glucose, L-glutamine, pyruvate), supplemented with L-glutamine (2.5 mM), penicillin 0.1 U mL^{-1} and streptomycin (0.1 μg mL^{-1}) and fetal bovine serum (10% v/v).

Extraction of fibroblasts from ear tissues. Euthanise mice (females BALB/cJRj) according to European Union un guidelines. Cut de ears and incubate during 5 min inf Ethanol 70%. In sterile conditions, allow the ethanol to air dry and remove any hair that may remain in the ears. Transfer the ears (10 units) into a 10 cm Petri dish containing 10 mL of digestion solution and cat the ears in pieces as small as possible. Incubate the digestion solution and ears during 90 minutes at 37 °C. Pipette up and down the digested tissue to homogenise and filter the cell suspension through a 70 μm filter and wash the undigested pellet with 10 mL of culture medium and complete the digestion mechanically. Centrifuge (600*g*, 20 min, 4 °C) the filtrate and remove the supernatant. Resuspend the pellet in 10 mL of medium and centrifuge again (centrifuge 3 times). Finally add 10 mL of media and transfer the cell suspension into culture flask (75 cm^2). Incubate the flak at 37 °C and 5% CO_2 for 3 days. After this time, the fibroblasts will adhere, and the cell debris will be floating. Remove medium and incubate for 24 h and the primary culture of fibroblast are ready.

MTT assay

Cell metabolic activity was analysed by an MTT-reduction assay to assess the primary fibroblasts sensitivity to the complexes. Thus, 5000 cells (fibroblast) per mL were seeded in flat-bottom 96-well plates (100 μL per well) in complete medium and allowed to attach for 24 h. A stock solution of the complexes was prepared in DMSO 0.1 M. Subsequent dilutions of the different stock solutions from the complexes using DMEM were prepared. 100 μL per well were added to the cells, in concentrations ranging from 0.1 to 50 μM (final concentration DMSO 0.1%) each concentration was performed by quadruplicate. Cells were cultured for a total of 72 h. 10 μL of MTT (5 mg ml^{-1} in PBS) were added to each well and then further 2 h incubation was allowed at 37 °C. Finally, after removing the culture medium, DMSO (100 μL per well) was added to dissolve the formazan crystals. A 96-well FLUOstar Omega (BMG LABTECH) was used to determine the optical density at 550 nm, and the IC_{50} was calculated. Each experiment was repeated in at least three independent analyses.

Cellular uptake studies. ICP-MS measurements was recorded in a PerkinElmer SCIEX ICP Mass spectrometer ELAN DRC-e with a sample flow of 1 mL min^{-1} and Rh as internal standard.

Samples were prepared as follows: 1 10^5 cells per well were seeded in a 12-well plate and incubated for 24 hours. Before adding the compounds, the culture medium was removed and then 2 mL of 0.4 μM (0.05% DMSO) of **3** and **4** were added. For the control, 2 mL of medium and 0.05% DMSO were added. Cells were incubated in the presence of compound for 48 h. The culture medium was then removed and 200 μL of trypsin was added to detach the cells and incubate 5 min then 800 μL of medium was added and cells were counted and a cell density of 6 10^4 cells per mL was found. Samples were centrifuged and the supernatant was removed. The digestion was carried out with 1 mL of HNO_3 : HCl (1 : 3) for 24 hours. Once the pellet was digested, 9 mL of ultrapure water was added, and ICP-MS measurements were performed in triplicate.

DNA binding

UV-vis titration experiments. In DNA binding experiments, the complexes were dissolved in DMSO and diluted with the Tris-HCl buffer (10 mM, pH = 7.4). The absorption spectra were performed in fixed concentration of metal complexes (20 μM) while gradually increasing the concentration of CT-DNA with 0 to 100 μM. To obtain the absorption spectra, the required amount of CT-DNA was added to both compound solution and the reference solution to eliminate the absorbance of CT-DNA itself. Each sample solution was allowed to equilibrate 5 min before the spectra was recorded. Using the absorption titration data, the binding constant K_b was determined using the Wolfe-Shimer equation:[37]

$$\frac{[DNA]}{(\varepsilon_a - \varepsilon_f)} \frac{[DNA]}{(\varepsilon_a - \varepsilon_f)} \frac{1}{K_b(\varepsilon_b - \varepsilon_f)}$$

where [DNA] is the concentration of CT-DNA, ε_a corresponds to the extinction coefficient observed (A_{obsd}/[M]), ε_f corresponds

to coefficient of free compound, ε_b is the extinction coefficient of the compound fully bound to CT-DNA, and K_b is the intrinsic binding constant. The K_b value was given by the ratio of slope to intercept in the plot of [DNA]/($\varepsilon_a - \varepsilon_f$) *versus* [DNA].

Competitive assay of fluorescence quenching. Fluorescence experiments were recorded in FluoTime300 PicoQuant spectrometer using a 1 cm path length quartz cuvette. Excitation wavelength for ethidium bromide was 525 nm and the titration experiments were recorded at 298 K. ctDNA solution in Tris/HCl (0.1 M, pH 7.2) was prepared with a concentration of 1 mg mL^{-1} and its molar concentration was measured using a Jasco V-780 UV–visible Spectrophotometer, resulting in 2.5 mM. Ethidium bromide and ctDNA solution was prepared in 2 mL Tris/HCl (0.1 M, pH 7.2) to a final concentration of 10 μM of EB and 50 μM of ctDNA. Then, successive additions of 20 μL of a solution of compound **3** or **4** [2 mM in DMSO] were performed.

TrxR inhibition. To determine the inhibition of mammalian TrxR, an established microplate-reader-based assay was performed. For this purpose, commercially available rat liver TrxR (from Sigma-Aldrich) was used and diluted with distilled water to achieve a concentration of 2 UmL^{-1}. The compounds were freshly dissolved as stock solutions in DMF. Aliquots (25 mL) of the enzyme solution and either potassium phosphate buffer (25 mL; pH 7.0) containing the compounds in graded concentrations or buffer (25 mL) without the compounds but DMF (positive control) were added. A blank solution (DMF in buffer; 50 mL) was also prepared (final concentrations of DMF: 0.5% v/v). The resulting solutions were incubated with moderate shaking for 75 min at 37 °C in a 96-well plate. A portion (225 mL) of reaction mixture (10 ml of reaction mixture consists of 1.0 ml PBS 1.0 M, pH = 7.0, 0.20 mL EDTA solution (500 mM pH 7.5), 0.80 ml de 63 mM DTNB in ethanol, 0.10 ml de 20 mg mL^{-1} de BSA 0.05 ml de NADPH 48 mM and 7.85 mL distilled water) was added to each well and the reaction was immediately initiated. After thorough mixing, the formation of 5-TNB was monitored with a microplate reader at 405 nm ten times in 35 s intervals. The increase in 5-TNB concentration over time followed a linear trend ($r^2 \geq 0.90$), and the enzymatic activities were calculated as the slopes (increase in absorbance per second) thereof. For each tested compound, noninterference with the assay components was confirmed by a negative control experiment using an enzyme-free test solution. IC_{50} values were calculated as the concentration of the compound decreasing the enzymatic activity of the untreated control by 50% and are given as the means and error of three repeated experiments.

Flow cytometry. 300 000 cells (MDA-MB-231) per mL were seeded in flat-bottom 6-well plates (1 mL per well) in complete medium and allowed to attach for 24 h. A solution of the complexes (**3** or **4**) was added at concentration of 4 × IC_{50} and cells were cultured for a total of 48 h. The cells were then deadhered with 200 μL of trypsin and resuspended in 1 mL of media. This cell suspension has been used for all flow cytometry measurements that have been carried out at cytometer SA3800 Sony (cell cycle) and cytometer GALLIOS Beckman Coulter. Commercial kits were used for all flow cytometry studies and in all cases, they were used as indicated in the manufacturer's instructions. Cell death studies: ANNEXIN V FITC Apoptosis detection kit (immunostep, reference ANXVKF-100T). Cell cycle: PI/RNASE Solution 200 test (immunostep, reference PI/RNASE). ROS production: CellROX® Green and CellROX® Orange Flow Cytometry Assay Kits (molecular probes by life technologies, catalogue number C10492). Mitochondrial potential: MitoStep™ Flow Cytometry Mitochondrial Membrane Potential Assay (immunostep, reference: MITO-100T).

Data availability

The supporting data for this article is provided in the ESI† section of this manuscript.

Conflicts of interest

The authors declare that they have no known competing financial interests or personal relationships that could have appeared to influence the work reported in this paper.

Acknowledgements

The authors thank projects PID2022-136861NB-I00 and PID PID2022-139739NB-I00 funded by MICIU/AEI10.13039/501100011033 and Gobierno de Aragón (Research Group E07_23R) for financial support of our research. The authors would also like to acknowledge the Spanish network, Organometallic Chemistry for Sustainable Solutions–OASIS (RED2022-134074-T). M. G.-M. acknowledges support by a Margarita-Salas Fellowship (European Union, NextGenerationEU). We thank E. Romanos for his help in the preparation of the primary lymphocytes.

References

1 I. Yousuf and M. Bashir, *Advances in Metallodrugs*, John Wiley & Sons, Ltd, 2020, pp. 1–39.
2 M. Shahlaei, S. M. Asl, A. Derakhshani, L. Kurek, J. Karges, R. Macgregor, M. Saeidifar, I. Kostova and A. A. Saboury, Platinum-based drugs in cancer treatment: Expanding horizons and overcoming resistance, *J. Mol. Struct.*, 2024, **1301**, 137366.
3 F. H. Abdalbari and C. M. Telleria, The gold complex auranofin: new perspectives for cancer therapy, *Discover Oncol.*, 2021, **12**, 42.
4 Y. Lu, X. Ma, X. Chang, Z. Liang, L. Lv, M. Shan, Q. Lu, Z. Wen, R. Gust and W. Liu, Recent development of gold(I) and gold(III) complexes as therapeutic agents for cancer diseases, *Chem. Soc. Rev.*, 2022, **51**, 5518–5556.

5 R. T. Mertens, S. Gukathasan, A. S. Arojojoye, C. Olelewe and S. G. Awuah, Next Generation Gold Drugs and Probes: Chemistry and Biomedical Applications, *Chem. Rev.*, 2023, **123**, 6612–6667.
6 M. Mora, M. C. Gimeno and R. Visbal, Recent advances in gold-NHC complexes with biological properties, *Chem. Soc. Rev.*, 2019, **48**, 447–462.
7 B. Bertrand, M. R. M. Williams and M. Bochmann, Gold(III) Complexes for Antitumor Applications: An Overview, *Chem. – Eur. J.*, 2018, **24**, 11840–11851.
8 G. Moreno-Alcántar, P. Picchetti and A. Casini, Gold Complexes in Anticancer Therapy: From New Design Principles to Particle-Based Delivery Systems, *Angew. Chem., Int. Ed.*, 2023, **62**, e202218000.
9 I. Ott, On the medicinal chemistry of gold complexes as anticancer drugs, *Coord. Chem. Rev.*, 2009, **253**, 1670–1681.
10 M. Gil-Moles, M. E. Olmos, M. Monge, M. Beltrán-Visiedo, I. Marzo, J. M. López-de-Luzuriaga and M. C. Gimeno, Silver-based Terpyridine Complexes as Antitumor Agents, *Chem. – Eur. J.*, 2023, **29**, e202300116.
11 A. Winter, M. Gottschaldt and R. George, Newkome and Ulrich S. Schubert, Terpyridines and their Complexes with First Row Transition Metal Ions:Cytotoxicity, Nuclease Activity and Self-Assembly of Biomacromolecules, *Curr. Top. Med. Chem.*, 2012, **12**, 158–175.
12 K. Malarz, D. Zych, M. Kuczak, R. Musioł and A. Mrozek-Wilczkiewicz, Anticancer activity of 4′-phenyl-2,2′:6′,2″-terpyridines - behind the metal complexation, *Eur. J. Med. Chem.*, 2020, **189**, 112039.
13 K. Choroba, B. Machura, A. Szlapa-Kula, J. G. Malecki, L. Raposo, C. Roma-Rodrigues, S. Cordeiro, P. V. Baptista and A. R. Fernandes, Square planar Au(III), Pt(II) and Cu(II) complexes with quinoline-substituted 2,2′:6′,2″-terpyridine ligands: From in vitro to in vivo biological properties, *Eur. J. Med. Chem.*, 2021, **218**, 113404.
14 S. Radisavljević, A. Kesić, D. Ćoćić, V. Marković, J. Milovanović, B. Petrović and A. R. Simović, New gold(III) chlorophenyl terpyridine complex: Biomolecular interactions and anticancer activity against human oral squamous cell carcinoma, *Appl. Organomet. Chem.*, 2023, **37**, e6922.
15 P. Shi, Q. Jiang, Y. Zhao, Y. Zhang, J. Lin, L. Lin, J. Ding and Z. Guo, DNA binding properties of novel cytotoxic gold (III) complexes of terpyridine ligands: the impact of steric, electrostatic effects, *J. Biol. Inorg. Chem.*, 2006, **11**, 745–752.
16 K. Czerwińska, M. Golec, M. Skonieczna, J. Palion-Gazda, D. Zygadło, A. Szlapa-Kula, S. Krompiec, B. Machura and A. Szurko, Cytotoxic gold(III) complexes incorporating a 2,2′:6′,2″-terpyridine ligand framework - the impact of the substituent in the 4′-position of a terpy ring, *Dalton Trans.*, 2017, **46**, 3381–3392.
17 M. Gil-Moles and M. C. Gimeno, The Therapeutic Potential in Cancer of Terpyridine-Based Metal Complexes Featuring Group 11 Elements, *ChemMedChem*, 2024, e202300645.
18 J. E. Aguado, M. J. Calhorda, M. C. Gimeno and A. Laguna, Unprecedented eta3-M3 coordination mode in a terpyridine ligand, *Chem. Commun.*, 2005, 3355–3356.
19 J. E. Aguado, M. C. Gimeno, P. G. Jones and A. Laguna, Unusual coordination behaviour of the ferrocenyl-terpyridine ligand with group 11 complexes, *Can. J. Chem.*, 2009, **87**, 341–347.
20 M. C. Gimeno, J. M. López-de-Luzuriaga, E. Manso, M. Monge, M. E. Olmos, M. Rodríguez-Castillo, M.-T. Tena, D. P. Day, E. J. Lawrence and G. G. Wildgoose, Synthesis, Photochemical, and Redox Properties of Gold(I) and Gold(III) Pincer Complexes Incorporating a 2,2′:6′,2″-Terpyridine Ligand Framework, *Inorg. Chem.*, 2015, **54**, 10667–10677.
21 M. Sirajuddin, S. Ali, A. Haider, N. A. Shah, A. Shah and M. R. Khan, Synthesis, characterization, biological screenings and interaction with calf thymus DNA as well as electrochemical studies of adducts formed by azomethine [2-((3,5-dimethylphenylimino)methyl)phenol] and organotin(IV) chlorides, *Polyhedron*, 2012, **40**, 19–31.
22 M. Sirajuddin, S. Ali, N. A. Shah, M. R. Khan and M. N. Tahir, Synthesis, characterization, biological screenings and interaction with calf thymus DNA of a novel azomethine 3-((3,5-dimethylphenylimino)methyl)benzene-1,2-diol, *Spectrochim. Acta, Part A*, 2012, **94**, 134–142.
23 M. Sirajuddin, S. Ali and A. Badshah, Drug-DNA interactions and their study by UV-Visible, fluorescence spectroscopies and cyclic voltametry, *J. Photochem. Photobiol., B*, 2013, **124**, 1–19.
24 V. T. Yilmaz, E. Gocmen, C. Icsel, M. Cengiz, S. Y. Susluer and O. Buyukgungor, Di- and polynuclear silver(I) saccharinate complexes of tertiary diphosphane ligands: synthesis, structures, in vitro DNA binding, and antibacterial and anticancer properties, *J. Biol. Inorg. Chem.*, 2014, **19**, 29–44.
25 S. Ramakrishnan, V. Rajendiran, M. Palaniandavar, V. S. Periasamy, B. S. Srinag, H. Krishnamurthy and M. A. Akbarsha, Induction of cell death by ternary copper (II) complexes of L-tyrosine and diimines: role of coligands on DNA binding and cleavage and anticancer activity, *Inorg. Chem.*, 2009, **48**, 1309–1322.
26 S. Gromer, L. D. Arscott, C. H. Williams, R. H. Schirmer and K. Becker, Human placenta thioredoxin reductase. Isolation of the selenoenzyme, steady state kinetics, and inhibition by therapeutic gold compounds, *J. Biol. Chem.*, 1998, **273**, 20096–20101.
27 (*a*) J. Bai, Y. Li and G. Zhang, Cycle regulation and anticancer drug discovery, *Cancer Biol Med.*, 2017, **14**, 348–362; (*b*) J Chen, The Cell-Cycle Arrest and Apoptotic Functions of p53 in Tumor Initiation and Progression, *Cold Spring Harbor Perspect. Med.*, 2016, **1**(6), a026104.
28 (*a*) Y. Jiang, X. Wang and D. Hu, Furanodienone induces G0/G1 arrest and causes apoptosis via the ROS/MAPKs-mediated caspase dependent pathway in human colorectal cancer cells: a study in vitro and in vivo, *Cell Death Dis.*, 2017, **8**, e2815; (*b*) K. Thangaraj, B. Balasubramanian, S. Park, K. Natesan, W. Liu and V. Manju, Orientin induces G0/G1 cell cycle arrest and mitochondria mediated intrinsic apoptosis in human colorectal carcinoma HT29 cells, *Biomolecules*, 2019, **9**, 418.

29 (*a*) K. Bhattacharya, A. K. Bag, R. Tripathi, S. K. Samanta, B. C. Pal, C. Shaha and C. Mandal, Mahanine a novel mitochondrial complex-III inhibitor induces G0/G1 arrest through redox alteration-mediated DNA damage response and regresses glioblastoma multiforme, *Am. J. Cancer Res.*, 2014, **4**, 629–647; (*b*) W. Li, G. B. Jiang, J. H. Yao, X. Z. Wang, J. Wang, B. J. Han, Y. Y. Xie, G. J. Lin, H. L. Huang and Y. J. Liu, Ruthenium(II) complexes: DNA-binding, cytotoxicity, apoptosis, cellular localization, cell cycle arrest, reactive oxygen species, mitochondrial membrane potential and western blot analysis, *J. Photochem. Photobiol., B*, 2014, **140**, 94–104; (*c*) S. Şimşek, A. A. Şüküroğlu, D. Yetkin, B. Özbek, D. Battal and R. Genç, DNA-damage and cell cycle arrest initiated anti-cancer potency of super tiny carbon dots on MCF7 cell line, *Sci. Rep.*, 2020, **10**, 13880.

30 A. Q. Khan, K. Rashid, A. A. AlAmodi, M. V. Agha, S. Akhtar, I. Hakeem, S. S. Raza and S. Uddin, Reactive oxygen species (ROS) in cancer pathogenesis and therapy: An update on the role of ROS in anticancer action of benzophenanthridine alkaloids, *Biomed. Pharmacother.*, 2021, **143**, 112142.

31 C. Musicco, A. Signorile, V. Pesce, P. Loguercio Polosa and A. Cormio, Mitochondria deregulations in cancer offer several potential targets of therapeutic interventions, *Int. J. Mol. Sci.*, 2023, **24**, 10420.

32 A. Bindoli, M. P. Rigobello, G. Scutari, C. Gabbiani, A. Casini and L. Messori, Thioredoxin reductase: A target for gold compounds acting as potential anticancer drugs, *Coord. Chem. Rev.*, 2009, **253**, 1692–1707.

33 E. C. Constable, C. E. Housecroft, M. Neuburger, A. G. Schneider, B. Springler and M. Zehnder, Programmed assembly of heteromultinuclear complexes using 4′-diphenylphosphino-2,2′:6′,2″-terpyridine, *Inorg. Chim. Acta*, 2000, **300–302**, 49–55.

34 R. Rubbiani, L. Salassa, A. de Almeida, A. Casini and I. Ott, Cytotoxic gold(I) N-heterocyclic carbene complexes with phosphane ligands as potent enzyme inhibitors, *ChemMedChem*, 2014, **9**, 1205–1210.

35 R. Rubbiani, I. Kitanovic, H. Alborzinia, S. Can, A. Kitanovic, L. A. Onambele, M. Stefanopoulou, Y. Geldmacher, W. S. Sheldrick, G. Wolber, A. Prokop, S. Wölfl and I. Ott, Benzimidazol-2-ylidene gold(I) complexes are thioredoxin reductase inhibitors with multiple antitumor properties, *J. Med. Chem.*, 2010, **53**, 8608–8618.

36 M. Khan and S. Gasser, Generating Primary Fibroblast Cultures from Mouse Ear and Tail Tissues, *J. Visualized Exp.*, 2016, **107**, e53565.

37 A. Wolfe, G. H. Shimer and T. Meehan, Polycyclic aromatic hydrocarbons physically intercalate into duplex regions of denatured DNA, *Biochemistry*, 1987, **26**, 6392–6396.